Dynamics of the dissipation range for solar wind magnetic fluctuations

Robert J. Leamon,[1] Norman F. Ness,[1] Charles W. Smith[1]
and
Hung K. Wong[2]

[1]*Bartol Research Institute, University of Delaware, Newark, DE*
[2]*Aurora Science Inc., San Antonio, TX*

Abstract. The dissipation range of interplanetary magnetic field (IMF) fluctuations is perhaps the least-studied aspect of the IMF. This is undoubtedly due, at least in part, to the large volume of data required to perform thorough studies of the high-frequency spectrum. We examine the properties of the dissipation range at 1 AU as observed by the WIND spacecraft, which include: (1) a general steepening of the power spectrum at spacecraft-frame frequencies comparable to, but greater than, the proton cyclotron frequency; (2) magnetic fluctuations that are largely transverse to the mean magnetic field, but less transverse than is seen in the high-frequency extent of the inertial range; (3) significant, but not maximal helicity and polarization signatures that indicate that ion-resonant dissipation is contributing to the magnetic spectrum; (4) a dominant fraction of the total magnetic energy is associated with wavevectors at large angles to the mean magnetic field; and (5) strong plasma β effects in the above results. In addition, we present a comparison of the observed onset of dissipation with a theory based on Kinetic Alfvén waves.

INTRODUCTION

This paper is a distillation of 3 previous papers of ours (1, 2, 3) on various aspects of the dissipation range of interplanetary fluctuations. See also the preceding Leamon *et al.* paper in this volume. These papers use for observations a collection of 83 hour-long intervals of WIND magnetic field and thermal plasma data: 33 of these events are in the quiet solar wind; the other 50 events are contiguous through the January 1997 coronal mass ejection. An example power spectrum for IMF fluctuations at 1 AU can be seen in Figure 1. At 0.24 Hz the spectrum sharply breaks from a Kolmogoroff-predicted $f^{-5/3}$ spectrum to a steeper f^{-3} spectrum; this steepened spectral form is identified as the dissipation range.

The ambient field and plasma parameters for the 1-hour interval whose spectrum shown in Figure 1 are all typical values for those parameters in the solar wind at 1 AU. This is, in part, why we use this one particular interval as an example.

Note that the spectral break frequency is comparable to, but greater than the proton gyrofrequency $\Omega_p/2\pi$. This association is seen for all the intervals we have studied (1, Figure 3). Together with the observation of an apparent depletion of outward-propagating Alfvén waves at frequencies above the proton gyrofrequency, this suggests cyclotron-resonant damping of Alfvén waves as the leading candidate for explaining the onset of the dissipation range.

If dissipation sets in at some wavevector $\mathbf{k}$, we may Doppler shift that wavevector into a spacecraft-frame frequency ν_{sc}:

$$\nu_{sc} = \frac{\mathbf{k}\cdot\mathbf{V}_{SW}}{2\pi} + \frac{\omega}{2\pi}, \qquad (1)$$

where $\mathbf{V}_{SW}$ is the solar wind velocity and ω the wave frequency. That $V_{SW} \gg v_A$, the Alfvén speed, implies that the first term on the RHS of equation 1 is greater than the second, at that in the plasma frame dissipation sets in at or above the cyclotron frequency.

The main conclusion of (1) was that the onset of the dissipation range could not be predicted using simple resonant theories for parallel-propagating Alfvén waves. This failure is independent of whether we assume that dissipation occurs either at some cylotron-resonant wavenumber, or at a wavenumber where γ/ω (ω and γ are the real and imaginary parts of the wave frequency, respectively) reaches some critical value. See the preceding Leamon *et al.* paper in this volume for a more involved reasoning and explanation of the inability of parallel-propagating Alfvén waves to predict the onset of the dissipation range.

The other evidence outlined in (1) against parallel-propagating waves is a test developed by Bieber *et al.* (4).

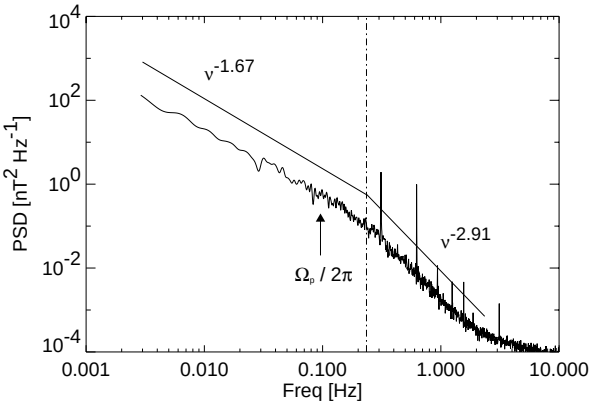

FIGURE 1. Trace of power spectral density matrix for hour 22UT, January 11, 1997, providing an example of a dissipation range power spectrum at 1 AU. For this period, $B = 6.27$ nT, $\beta_p = 0.480$, $\Theta_{BV} = 38.1°$, $V_{SW} = 517$ km s^{-1}, and $\Omega_p = 0.605$ rad s^{-1} (0.096 Hz). The spectral break frequency is computed to be 0.235 Hz. Spacecraft-generated spintones are seen at harmonics of 0.33 Hz and a noise signal exists above ~ 1 Hz.

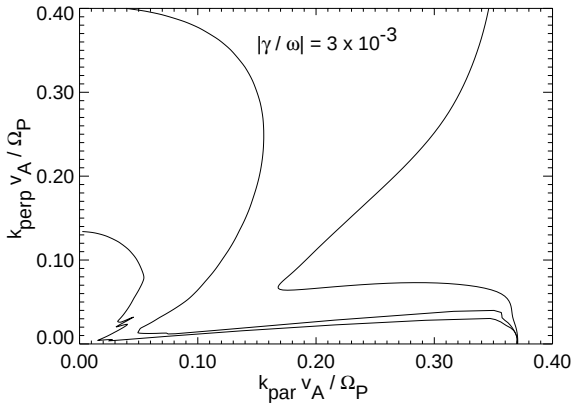

FIGURE 2. Demonstrating that electron resonance effects control the shape of the $|\gamma/\omega| = 3 \times 10^{-3}$ contour. All three contours have $\beta_p = 0.5$; from the outside in, the values of β_e for the three contours are 10^{-6}, 0.5 and 2.5.

Bieber assumes a two-component model wherein all fluctuations are either "slab" ($\mathbf{k} \parallel \hat{\mathbf{B}}$) or "2-D" ($\mathbf{k} \perp \hat{\mathbf{B}}$). The existence of a significant 2-D component was first put forward by Matthaeus *et al.* (5). The minimum-variance direction is field-aligned for both components. The ratio of the spectral power between components in the field-aligned coordinate system $(\hat{\mathbf{y}}, -\hat{\mathbf{x}}, \hat{\mathbf{z}}) = (\hat{\mathbf{B}} \times \hat{\mathbf{R}}, \hat{\mathbf{B}} \times (\hat{\mathbf{B}} \times \hat{\mathbf{R}}), \hat{\mathbf{B}})$, where $\hat{\mathbf{R}}$ is radially outwards, is related to the fraction of energy present in "slab" modes.

The results of this test are that, averaging over all the quiet solar wind intervals studied, 89% of the energy in the inertial range is contained in highly oblique modes, while in the dissipation range (at least in the first decade of frequency, before the signal becomes obscured by noise), this value falls to 54%. This result may be explained by the preferential dissipation of oblique modes.

There are three low-frequency, obliquely propagating electromagnetic wave modes. We discount the slow-mode wave and the fast magnetosonic wave as they are both heavily damped in a high-β plasma, throughout even the inertial range (6). However, the shear Alfvén wave becomes the Kinetic Alfvén wave (KAW) when $k_\perp R_L \sim 1$, where R_L is the Larmor radius, and it develops a parallel electric field component, which causes electron-Landau damping to become important. Ion cyclotron damping can also play a significant role if $\omega \sim \Omega_p$. Dissipation should occur, therefore, when $k_\perp R_L \sim 1$ or $k v_A / \Omega_p \sim 1$; thus the dissipation scale length associated with the KAW is quite consistent with the observed properties of the dissipation range.

In the rest of this paper we consider the oblique fluctuations to be KAWs, and test to see if these waves can explain the observed properties of the dissipation range.

SYNTHETIC KAW SPECTRA

We have a set of KAW solutions calculated via the linearized Vlasov-Maxwell equations. Based on these solutions we construct a sample 3-D spectrum $E(\mathbf{k})$ and test if the power law indices and abrupt break can be preserved when the 3-D form is reduced to a spacecraft-frame frequency spectrum $F(f)$. In this way we obtain a 3-D spectrum that is consistent with the observations, but not unique.

The details of this calculation are explained in (3), but we shall summarise them here. We take the whole set of KAW solutions for $\beta = 0.5$ (recall that $\beta_p = 0.48$ for the interval in Figure 1), and assume that dissipation sets in at some contour of constant γ/ω. We acknowledge that at first glance this appears to be an *ad hoc* assumption, but does make sense on a number of timescale-based arguments (3). For values of k "inside" this contour the spectrum falls as $k^{-11/3}$, and outside the contour the spectrum falls as k^{-5}, so that the reduced 1-D power spectrum will have spectral indices of $-5/3$ and -3 if the spectrum reduces correctly. The spectrum is azimuthally symmetric about $\mathbf{B}_0$; the only anisotropy present is that which arises from the dissipation contour.

Sample contours for the KAW dispersion relations are shown in Figure 2 as functions of $k_\parallel$ and $k_\perp$. There is a distinctive two-lobed structure with a strong cusp at $\theta_{kB} \sim 20°$. Increasing β_e changes the oblique lobe much

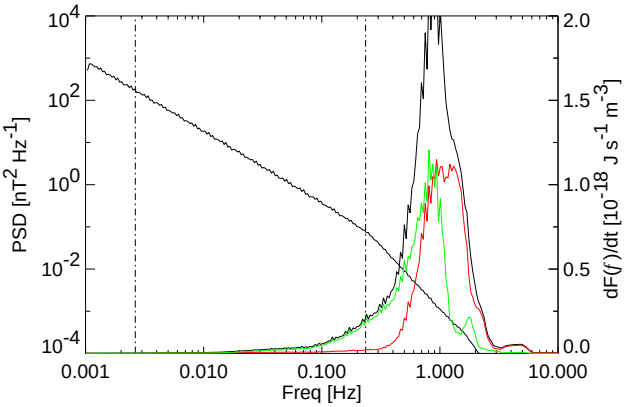

FIGURE 3. Synthetic power spectrum of Kinetic Alfvén waves (left-hand scale) and heating rate $dF(f)/dt$ as a function of frequency. The total heating rate, which is the sum over all of the 250 logarithmically-spaced frequency bins used, is 6.36×10^{-17} J s^{-1} m^{-3}. Under the heating rate curve are the electron and proton contributions, at slightly lower and higher frequencies, respectively.

more than the parallel lobe. We infer, therefore, that ion-cyclotron resonance dominates dissipation for small angles, but electron-Landau damping dominates above the cusp.

Having constructed our synthetic 3-D spectrum $E(\mathbf{k})$, we now reduce it to a Doppler-shifted frequency spectrum according to

$$F(f) = \int E(\mathbf{k})\,\delta\left(\frac{1}{2\pi}\left(\mathbf{k}\cdot\mathbf{V}_{SW} + \omega(\mathbf{k})\right) - f\right) d\mathbf{k} \quad (2)$$

where $\omega(\mathbf{k})$ is the real part of the wave frequency determined from the linear Vlasov-Maxwell solutions, $\delta(\ldots)$ is the Dirac delta function, f is the spacecraft-frame frequency, and for $\mathbf{V}_{SW}$ we take the observed solar wind velocity for the interval in question. The results of this reduction can be seen on the left-hand scale of Figure 3. The spectrum does indeed correctly reduce to $-5/3$ and -3 power laws, and given a judicious choice of contour, the break in the spectrum is almost exactly reproduced. The break contour used in computing Figure 3 is $\gamma/\omega = 3 \times 10^{-3}$, which is why this contour value was used to illustrate Figure 2.

The peaked traces and right-hand scale of Figure 3 correspond to the rate at which damping of Kinetic Alfvén waves heats the background plasma. The heating rate (in J s^{-1} m^{-3}) is

$$\dot{Q} \sim 2\int E(\mathbf{k})\gamma(\mathbf{k})d\mathbf{k}. \quad (3)$$

By including a Dirac delta function similar to that in equation 2, we can see how this heating is distributed in frequency. The bulk of the heating occurs at dissipation range frequencies, peaking at $\simeq 1$ Hz. However, there is some heating in the inertial range of the spectrum, and this is due to the heating of electrons.

Perhaps surprisingly, the heating rate of the protons alone is only 57.5% of the total. Recall that the dominant mode of damping at high Θ_{BV} is electron-Landau damping. An even more significant implication of the calculated heating rate result is that it is about 3 times larger than that sufficient to match the *in situ* heating rate required by the non-adiabatic radial temperature profile of the solar wind (7). Again, see (3) for more details.

PREDICTION OF SPECTRAL BREAK FREQUENCY

We can see from Figure 3 how well our model of a 3-D spectrum of Kinetic Alfvén waves does at predicting the spectral break frequency, given a judicious choice of γ/ω for the contour. What remains to be seen is how well the model works for all the intervals we have studied. The method used to produce Figure 3 that consists of first calculating a k–θ contour for each interval (with the observed β_p) and each value of γ/ω, and constructing a fully 3-D $E(\mathbf{k})$ to be reduced to a frequency spectrum is rather labor-intensive. Instead, we use a "maximum projection" argument whereby we determine the wavevector lying on a contour of constant γ/ω for which $\mathbf{k}\cdot\mathbf{V}_{SW}$ is maximum, and this wavevector is then Doppler-shifted into the spacecraft frame to be the KAW-predicted frequency. This simple shortcut has been tested against the more detailed analyses of the previous section and verified (3).

The contour of constant γ/ω is varied by trial-and-error until the best-fit straight line through the data has unit slope. The left-hand panel of Figure 4 shows this result for $\gamma/\omega = 0.01$. Although the best-fit straight line is plotted, we do not believe that this line truly represents the data. The January 1997 magnetic cloud data (open circles) clearly form a separate population from the solar wind data, and these points affect the slope and intercept of the best-fit straight line. The best-fit line through all the data is clearly not the best fit to the solar wind data points.

We reject the validity of the left-hand panel of Figure 4 for a second reason: the angle between the mean field and the wavevector $\mathbf{k}$ for which $\mathbf{k}\cdot\mathbf{V}_{SW}$ is maximum is consistently in the range 60–80°. (There are only 4 events which are best modelled by "slab" waves, *i.e.*, $\theta_{kB} \lesssim 10°$.) As we have shown above, at these angles electron Landau damping and thus β_e dominates the shape of the contour. It would make sense then if we use β_e rather than β_p to

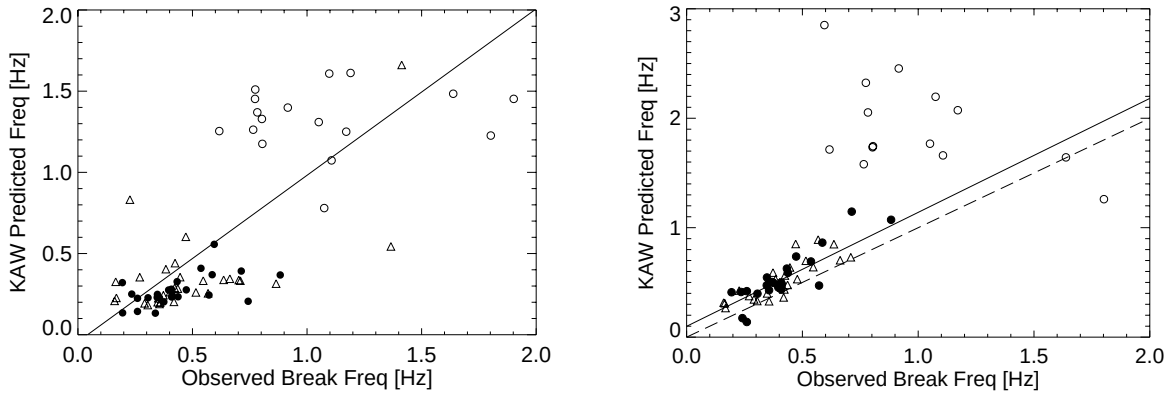

FIGURE 4. Plots of KAW-predicted spectral break frequency against observed break frequency. Left panel: Best-fit value of $\gamma/\omega = 0.01$. Quiet solar wind observations are shown as triangles, and January 1997 observations are circles. Open circles correspond to observations inside the magnetic cloud and filled circles correspond to solar wind observations before and after the CME. The solid line is best-fit straight line. Right panel: using β_e instead of β_p produces much tighter results. The solid line is the best-fit straight line through the data, excluding the magnetic cloud observations and the dashed line represents equality. The best-fit straight line again corresponds to the contour $\gamma/\omega = 0.01$. There are fewer data points on this panel because electron plasma data is not available for all the the intervals studied.

predict the onset of the dissipation range. This is precisely what is done to produce the right-hand panel of Figure 4. There is far less scatter of the points around the new best-fit straight line, which also corresponds to the contour $\gamma/\omega = 0.01$. Again, the angle θ_{kB} for which $\mathbf{k} \cdot \mathbf{V}_{SW}$ is maximum is consistently in the range 60–80°.

The geometry of magnetic fluctuations is much more two-dimensional in a magnetic cloud (2), so we must question the validity of our model of obliquely propagating Kinetic Alfvén waves inside magnetic clouds.

SUMMARY

The main conclusions of this paper are as follows:

1) Parallel-propagating "slab" Alfvén waves cannot explain the onset of the IMF dissipation range.

2) Up to 90% of the total magnetic fluctuation energy resides in wavevectors at large angles to the mean magnetic field.

3) Reducing a 3-D spectrum of Kinetic Alfvén waves not only correctly predicts the onset of the IMF dissipation range, but the total energy dissipated by $2\int E(\mathbf{k})\gamma(\mathbf{k})d\mathbf{k}$ is within a factor of 3 of that required by the (non-adiabatic) radial temperature profile.

4) Electron effects are important: β_e and electron-Landau resonance controls the onset of the IMF dissipation range at spatial scales comparable to the ion gyroradius. This is consistent with the observation that at these scales the waves become more compressive and have greater fluctuations in $|\mathbf{B}|$ (1, Figures 3 and 4). Also, β_e controls the heating rate of both protons and electrons, with about half the total energy dissipated going to heat thermal electrons.

This work is supported by the Wind mission through NASA subcontract NAG5-2848 to the Bartol Research Institute. The participation of H.K.W. is supported by NASA contract NAS5-32484 and by a grant to the Goddard Space Flight Center from the NASA Space Physics Theory Program.

REFERENCES

1. Leamon, R. J., C. W. Smith, N. F. Ness, W. H. Matthaeus, and H. K. Wong, *J. Geophys. Res.*, **103**, 4775–4787 (1998).
2. Leamon, R. J., C. W. Smith, and N. F. Ness, *Geophys. Res. Lett.*, **25**, 2505–2508 (1998).
3. Leamon, R. J., C. W. Smith, N. F. Ness, and H. K. Wong, Dissipation range dynamics: Kinetic Alfvén waves and the importance of β_e, *J. Geophys. Res.*, submitted (1998).
4. Bieber, J. W., W. Wanner, and W. H. Matthaeus, *J. Geophys. Res.*, **101**, 2511–2522 (1996).
5. Matthaeus, W. H., M. L. Goldstein, and D. A. Roberts, *J. Geophys. Res.*, **95**, 20 673–20 683 (1990).
6. Barnes, A., in *Solar System Plasma Physics*, **1**, edited by E. N. Parker, C. F. Kennel, and L. J. Lanzerotti, 249–319, North-Holland, New York (1979).
7. Richardson, J. D., K. I. Paularena, A. J. Lazarus, and J. W. Belcher, *Geophys. Res. Lett.*, **22**, 325–328 (1995).